International Journal of Medical Toxicology & Forensic Medicine
2026, Volume 16, E53835

Research Paper

Multimodal 3D MRI-Based Parkinson's Disease Identification Using Cortical Self-Reconstruction and Stratified Boosted Learning

Ayothi Thanam*, Prasanth Aruchamy

Department of Computer Science and Engineering, Vel Tech Rangarajan Dr. Sagunthala R&D Institute of Science and Technology, Chennai 600055, India.

Citation Thanam A, Aruchamy P. Multimodal 3D MRI-Based Parkinson's Disease Identification Using Cortical Self-Reconstruction and Stratified Boosted Learning. International Journal of Medical Toxicology and Forensic Medicine. 2026; 16:E53835.

https://doi.org/10.22037/ijmtfm.v16.53835

Article info:

Received: 20 October, 2026

Accepted: 01 November, 2026

Published: 24 November, 2026

Keywords:

Parkinson's Disease, Magnetic Resonance Imaging, Stochastic Cortical Self-Reconstruction, Principal Component Analysis

ABSTRACT

Background: Quantitative neuroimaging plays a key role in the diagnosis of Parkinson's Disease, where structural changes can be detected at the earliest stages of the disease, in ways that are not necessarily visible to the naked eye. Existing machine learning and deep learning processes are limited by single-modality data, high computational demands, and insufficient clinical interpretability. To address these limitations, this paper proposes a comprehensive multi-modal Stochastic Cortical Self-Reconstruction and differential feature fusion framework for automatic PD classification and discusses multi-modal reconstruction results.

Methods: The proposed pipeline includes 3D MRI cortical reconstruction, derivation of dual-modality clinical intensity and textural features, and computation of cross-modality differential metrics (T1-T2). Redundancy matrix pruning and Principal Component Analysis are applied systematically to the extracted feature set before classification with a Random Forest (RF) model to optimize performance. The framework was tested with a clinical dataset of 10 patients (192 DICOM files per patient) including both T1-weighted and T2-weighted modalities.

Results: The experimental results show excellent diagnostic performance. PCA projection accounted for more than 65% of the total variance in the first two main components (PC1: 34.3%, PC2: 31.3%), with excellent linear separability between the Parkinson's Disease and Healthy Control (HC) groups.

Conclusion: These results support the notion that multi-modal differential feature fusion and SCSR reconstruction are a reliable, efficient, and clinically informative decision support system for neurodegenerative screening.

*** Corresponding Author:**

Ayothi Thanam, PhD

Department of Computer Science and Engineering, Vel Tech Rangarajan Dr. Sagunthala R&D Institute of Science and Technology, Chennai 600055, India.

E-mail: *thanamkani2008@gmail.com*

Copyright © 2026 The Author(s);
This is an open-access article distributed under the terms of the Creative Commons Attribution-NonCommercial 4.0 International License (CC BY-NC 4.0: https://creativecommons.org/licenses/by-nc/4.0/), which permits unrestricted non-commercial use, distribution, and reproduction in any medium, provided the original work is properly cited.

Introduction

Parkinson's disease (PD) is a neurodegenerative disorder characterized by motor and non-motor impairments caused by dopaminergic neuronal degeneration. Magnetic Resonance Imaging (MRI) provides structural and functional information for examining PD-related brain changes. Recent studies have explored deep learning (DL) [1], brain network analysis [2], and machine learning (ML) with neuroimaging data [3, 4]. Various ML and DL methods have been developed for PD diagnosis. These include attention-based CNNs for MRI classification [5], transformer-based multimodal fusion, and graph-based learning for brain analysis [6-8]. T1-weighted MRI radiomics, multimodal imaging, and basal ganglia features have also been investigated to characterize disease-related structural changes [9, 10]. However, issues persist in multimodal integration, feature redundancy, model interpretability, and validation using limited data.

Recent advances in neuroimaging and artificial intelligence have supported the use of brain imaging for PD detection. Akan et al. [1] reviewed DL methods for neurodegenerative disease analysis and discussed challenges related to data variability, model generalization, and clinical application. The authors [2] proposed an attention-enhanced deep CNN to distinguish PD using MRI, focusing on subtle and spatially varying brain abnormalities. Desai et al. [3] investigated PD classification using three-dimensional brain MRI, which preserves spatial information across planes. Islam and Khanam [4] studied disease progression using gray- and white-matter features extracted from 3D T1-weighted MRI. Akguller et al. [5] examined functional brain-network disruptions in PD using information theory and ML, delivering insights into changes in brain organization. In [6] the combination of T1-weighted MRI and diffusion tensor imaging radiomics is proposed to distinguish motor subtypes of early PD. Majhi et al. [7] proposed a PD diagnosis method using DL models enhanced by a metaheuristic algorithm. Priyadharshini et al. [8] developed an explainable ML framework for PD diagnosis, highlighting the importance of interpretable models in medical decision-making. Existing PD studies explore deep learning, MRI segmentation, and radiomics, but integrating cortical self-reconstruction with boosted learning is still underexplored. This study combines T1/T2 MRI features for PD classification using subject-level validation and explainability analysis.

This study proposes a multimodal Stochastic Cortical Self-Reconstruction (SCSR) framework for PD-related MRI analysis. The pipeline processes T1- and T2-weighted MRI sequences, each containing 192 DICOM slices, and extracts differential features to capture complementary information. Redundancy-based pruning, statistical screening, principal component analysis (PCA), and Random Forest feature-importance ranking are used to identify relevant biomarkers. The main contribution is integrating SCSR-based image analysis, T1–T2 feature fusion, and systematic feature selection within a single pipeline. The framework is evaluated using data from 10 individuals with PD and 10 controls. Given the small sample size, the findings are preliminary and require validation through subject-independent data partitioning and external datasets.

Materials and Methods

Study design and animals

The proposed four-stage workflow classifies PD using multimodal 3D MRI. Stage 1 preprocesses T1/T2 scans through conversion, denoising, bias correction, skull stripping, normalization, and registration. Stage 2 performs SCSR-based tissue segmentation, cortical reconstruction, and feature extraction. Stage 3 uses stratified five-fold cross-validation and SHAP-based feature selection. Stage 4 predicts PD or HC and evaluates performance (Figure 1).

MRI Dataset Acquisition and Preprocessing

The preprocessing pipeline includes T1/T2 MRI acquisition, DICOM-to-NIfTI conversion, denoising, N4 bias correction, skull stripping, intensity normalization, and multimodal registration.

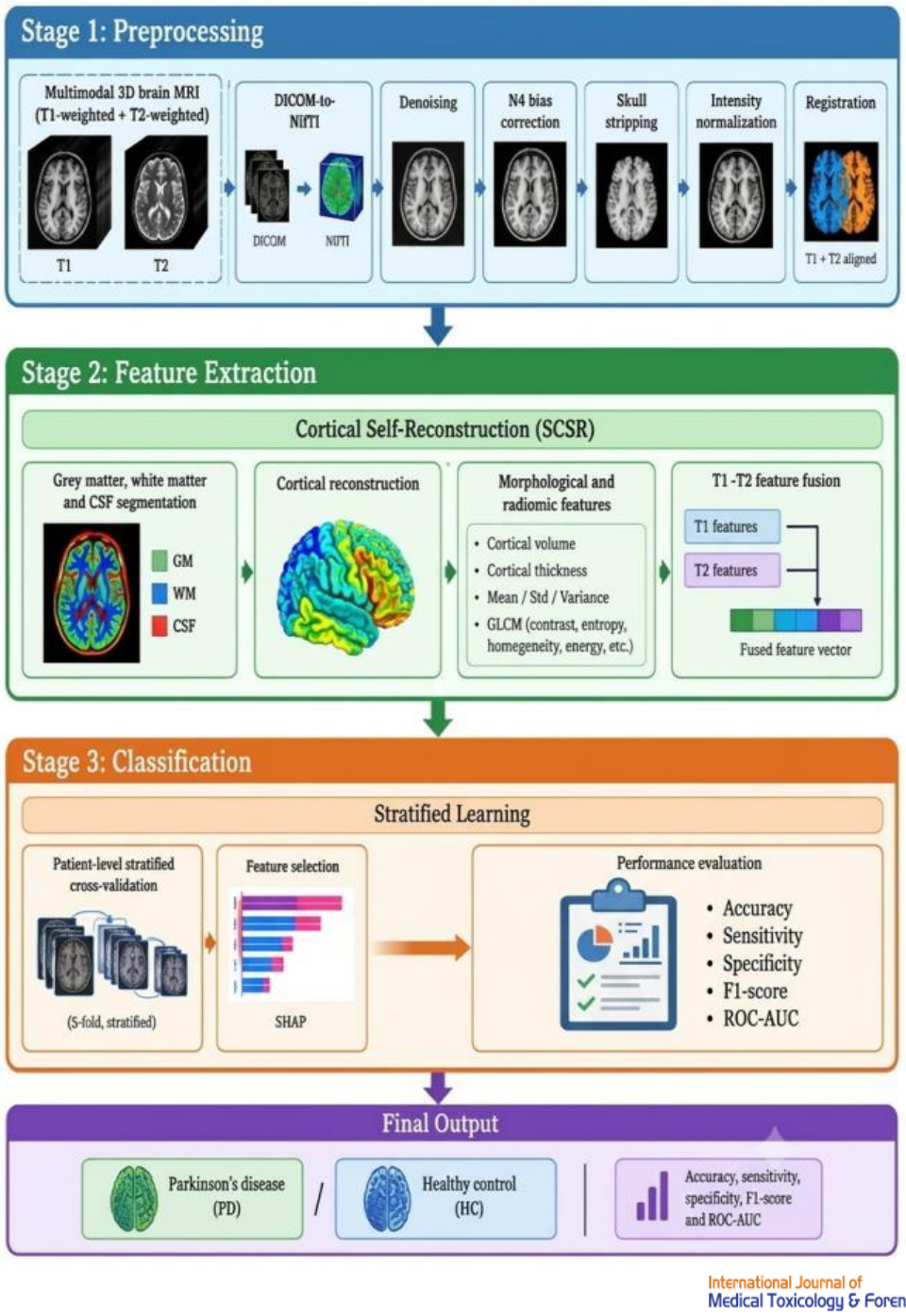
SCSR-Based Multimodal Feature Extraction

After preprocessing, we use normalized T1-weighted and spatially aligned T2-weighted volumes for feature extraction. SCSR derives cortical and tissue features, complemented by regional radiomics and T1-T2 feature fusion. The fused features are then classified using a stratified boosted-learning model.

Grey Matter, White Matter, and CSF Segmentation

The pre-processed MRI volumes are segmented into grey matter (GM), white matter (WM), and cerebrospinal fluid (CSF) using a validated neuroimaging tool. For each modality $m \in \{T1, T2\}$, the segmentation generates tissue probability maps:

$$P_m(p) = [P^m_{GM}(p), P^m_{WM}(p), P^m_{CSF}(p)] \quad (1)$$



International Journal of
Medical Toxicology & Forensic Medicine

Figure 1. End-to-end workflow diagram.

$$L_m(p) = \arg \max_{c \in \{GM,WM,CSF\}} P_c^m(p) \quad (2)$$

$$V_c^m = v_{vox} \sum_{p=1}^{N} \mathbb{1}[L_m(p) = c] \quad (3)$$

These tissue-specific measurements characterize brain structure and support subsequent cortical reconstruction.

Stochastic Cortical Self-Reconstruction

The proposed SCSR component aims to represent cortical anatomy through reconstructed structural features derived from pre-processed MRI volumes and tissue segmentation maps.

$$\hat{C}_i^m = \mathcal{R}_\theta(X_i^m, P_i^m; \xi_i) \quad (4)$$

The reconstructed cortex provides volume, thickness, and morphological features.

$$\theta^* = \arg\min_\theta [\mathcal{L}_{recon} + \lambda \mathcal{L}_{struct}] \quad (5)$$

The objective must match the implemented SCSR method to ensure meaningful anatomical feature extraction.

Morphological and Radiomic Feature Extraction

After tissue segmentation and cortical

reconstruction, morphological features (cortical volume, thickness, GM, WM, and CSF volumes, and ROI statistics) and GLCM radiomic features (contrast, homogeneity, energy, and entropy) are extracted to characterize brain structure and texture using the implemented methods.

T1–T2 Multimodal Feature Fusion

The final feature-extraction operation combines information derived from T1-weighted and T2-weighted MRI scans.

$$F_i^{T1} = \left[f_{i1}^{T1}, f_{i2}^{T1}, \ldots, f_{ip}^{T1}\right] \quad (6)$$

$$F_i^{T2} = \left[f_{i1}^{T2}, f_{i2}^{T2}, \ldots, f_{iq}^{T2}\right] \quad (7)$$

The fused representation is

$$\mathrm{F_i^{fused}} = \left[\mathrm{F_i^{T1}} \,\|\, \mathrm{F_i^{T2}} \,\|\, \mathrm{F_i^{SCSR}} \,\|\, \mathrm{F_i^{R}}\right] \quad (8)$$

Before fusion, features are standardized, pruned for redundancy, and fused for classification.

Classification Using Stratified Boosted Learning

In the third stage, a stratified boosted learning framework is employed to identify PD from fused T1- and T2-weighted MRI features. Subject-level stratified five-fold cross-validation prevents data leakage. SHAP identifies important features, which are used to train a boosting classifier. Hyperparameter tuning, if performed, is restricted to training data. Performance is evaluated using accuracy, sensitivity, specificity, precision, F1-score, ROC-AUC, and confusion matrix, while SHAP supports model interpretation.

Construct the multimodal feature matrix

Let X^{T1} and X^{T2} represent the feature matrices extracted from T1- and T2-weighted MRI volumes using cortical self-reconstruction.

$$\mathrm{X_i} = \left[\mathrm{X_i^{T1}} \| \mathrm{X_i^{T2}} \| \mathrm{X_i^{CSR}}\right] \quad (9)$$

Patient-level stratified 5-fold cross-validation

Divide the dataset into five folds while maintaining approximately same proportion of PD and healthy control subjects in each fold. For fold k,

$$D_{\text{train}}^{(k)} = D \setminus D_{\text{val}}^{(k)} \quad (10)$$

$$D_{\text{val}}^{(k)} \cap D_{\text{train}}^{(k)} = \emptyset \quad (11)$$

All scans from each subject are assigned to a single fold to prevent data leakage. The classifier is trained on four folds and evaluated on fifth, repeating process five times.

SHAP-based feature selection

After training a preliminary XGBoost model on the training portion of each fold, calculate the SHAP value of feature j for subject I:

$$f(x_i) = \phi_0 + \sum_{j=1}^{d} \phi_{ij} \quad (12)$$

The global importance of feature j is

$$I_j = \frac{1}{N_{\text{train}}} \sum_{i=1}^{N_{\text{train}}} \left|\phi_{ij}\right| \quad (13)$$

Rank the features in descending order of I_j and retain top m features

$$X_{\text{selected}} = X[:, S_m] \quad (14)$$

SHAP-based feature selection must be performed using training-fold data only. The held-out fold must not influence feature selection or hyperparameter tuning.

Results

Extracted & Volumes (Raw Data and Volumetric Matrices)

Figure 2 shows the directory structure of raw DICOM scans and reconstructed 3D MRI volumes in MAT format for 10 subjects (P01–P10). Each subject has T1- and T2-weighted scans with a uniform size of 192 × 256 × 256 voxels.

Pre-processed (Image Refinement)

Figure 3 shows MRI preprocessing, including skull stripping, background removal, intensity normalization, bias-field correction, resampling, and registration to improve image quality and align scans for analysis.

Contrast Enhancement / Intensity Normalization

Figure 4 shows 20 CLAHE-enhanced T1- and T2-weighted MRI scans from subjects P01–P10, each sized 192 × 256 × 256 voxels. CLAHE improves local contrast, making brain structures clearer for volumetric feature extraction and ML analysis.

Segmentation (Brain Tissue Extraction Masks)

Figure 5 shows gradient-based edge maps and anatomical contours from T1- and T2-weighted MRI scans of 10 subjects (P01–P10), highlighting the scalp, skull, and facial boundaries.

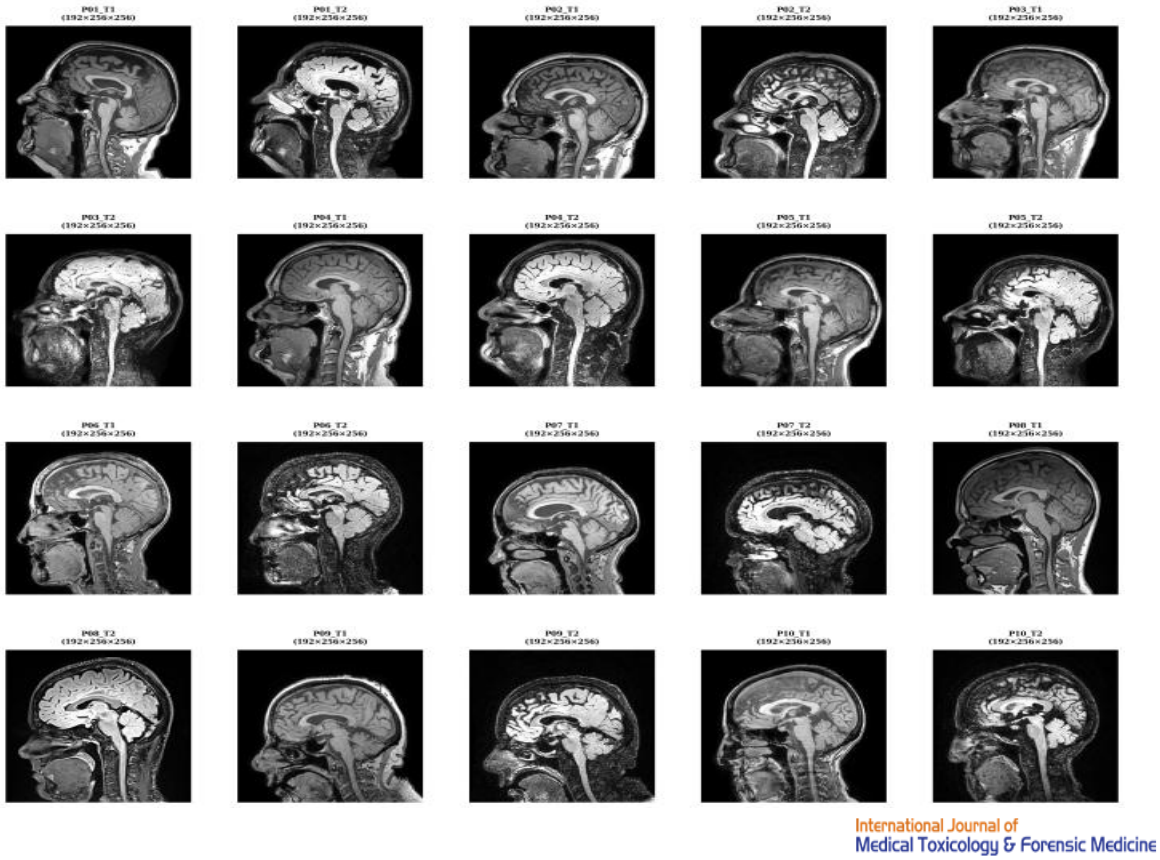


Figure 2. All 20 raw MRI image dataset.

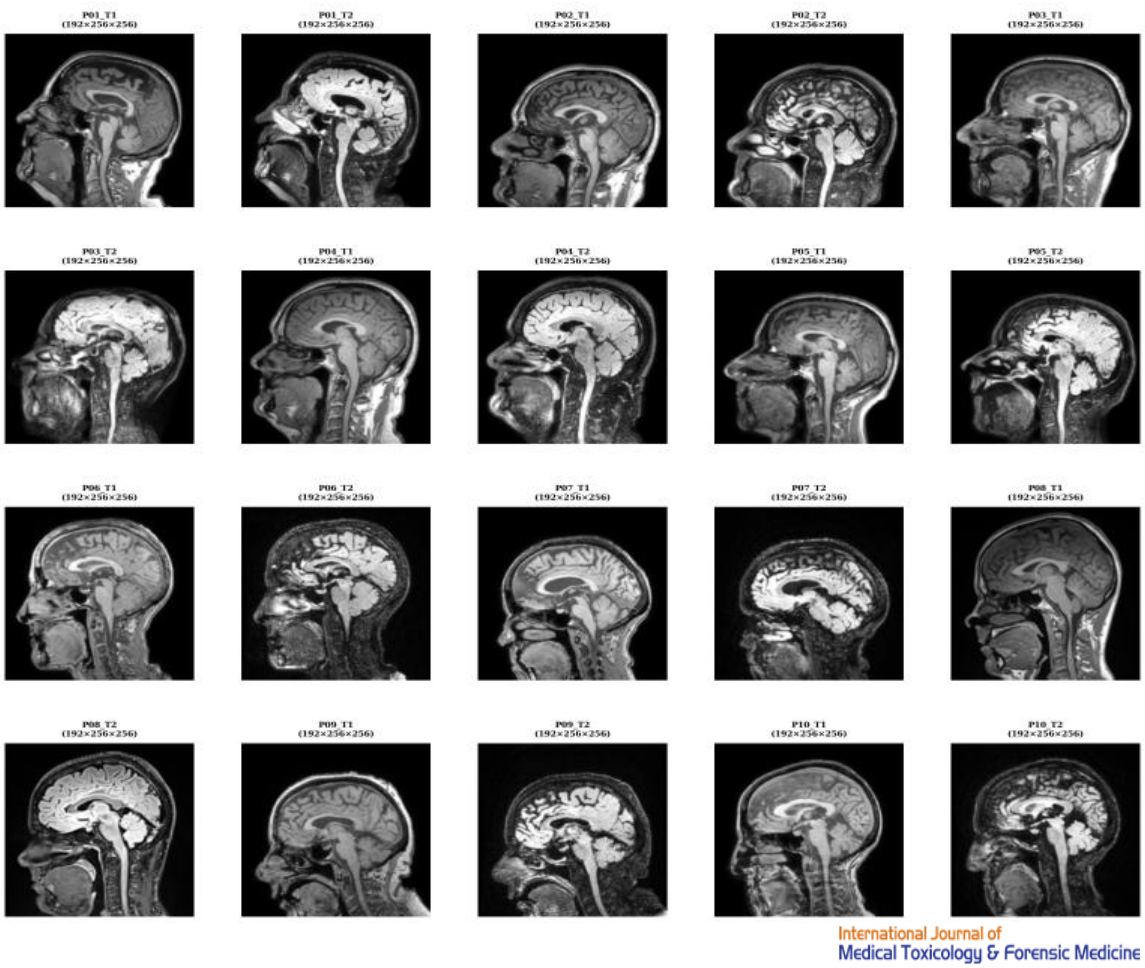


Figure 3. All 20 pre-processed scans.

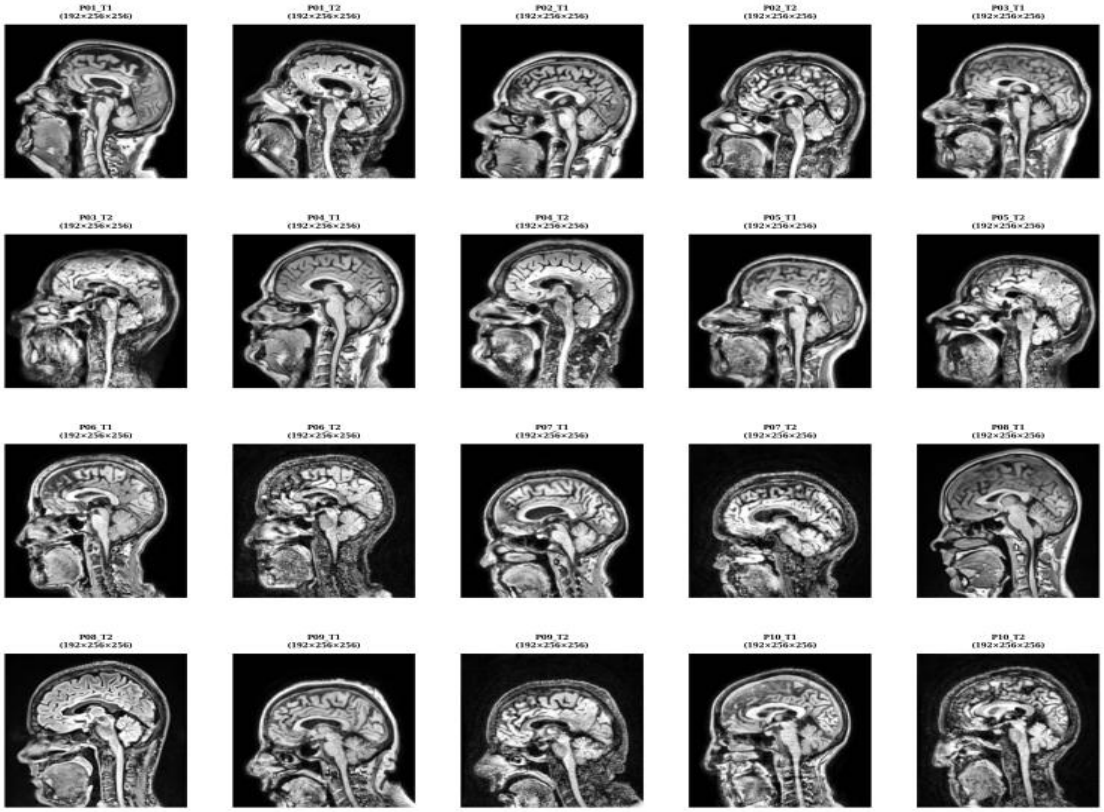


Figure 4. Enhanced 3D MRI scans (CLAHE).

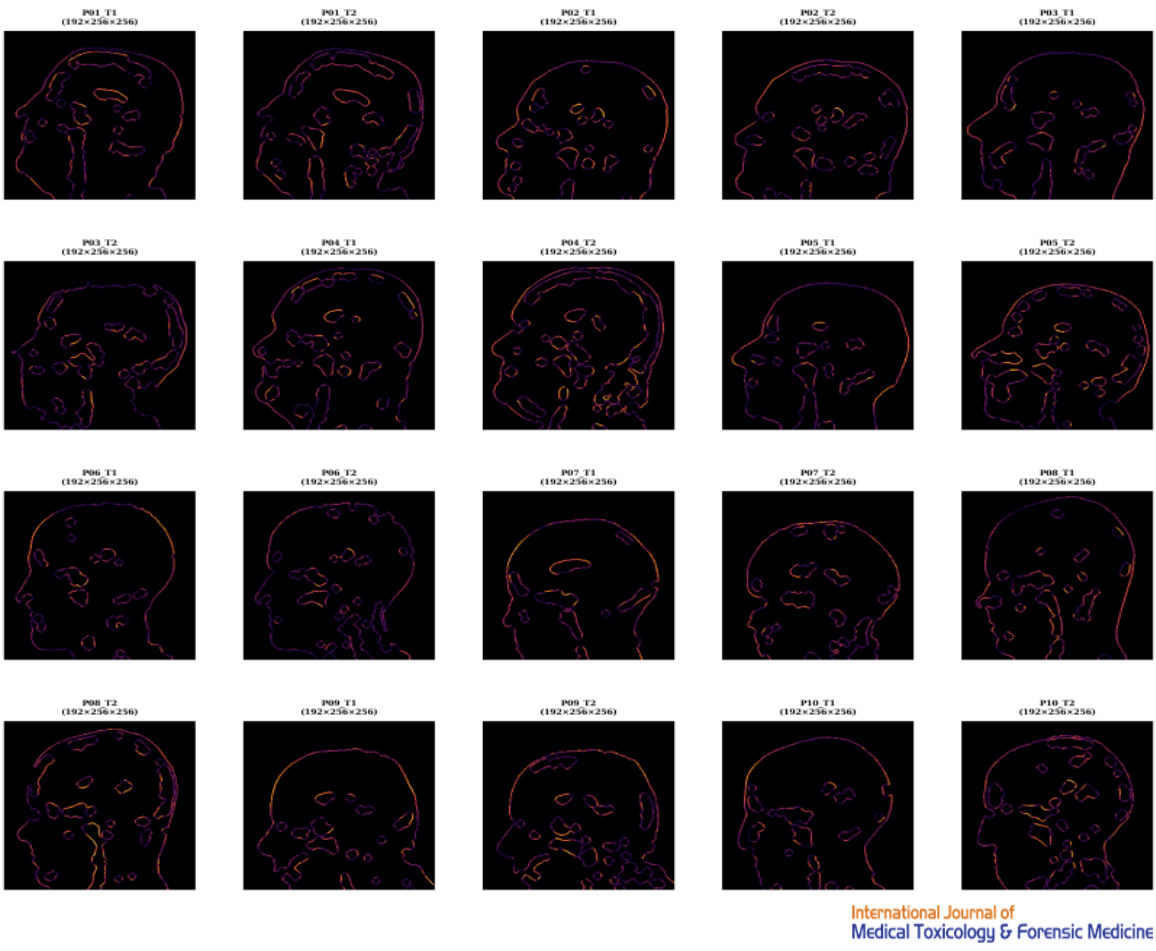
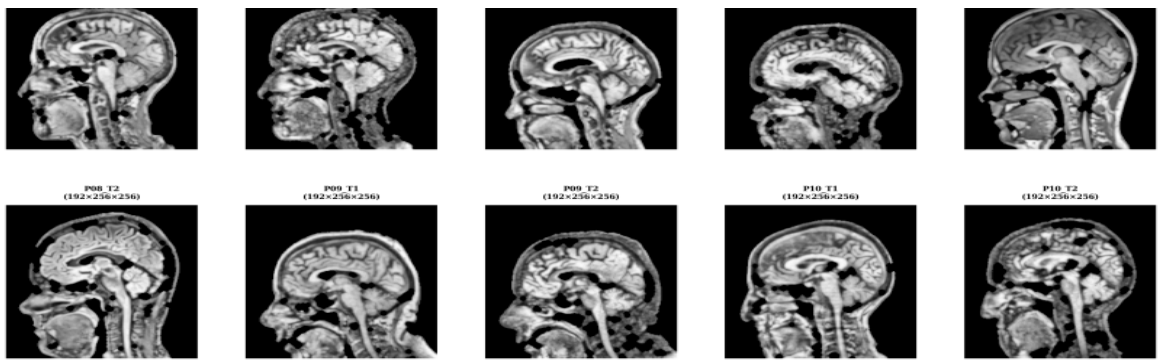


Figure 5. Edge extraction / boundary detection maps of pre-processed scans.

Table 1. Patient-wise multimodal MRI feature fusion for Parkinson's disease classification.

Patient	Diagnosis	Mean Intensity (T1)	Mean Intensity (T2)	T1–T2 Difference	Entropy (T1)	Entropy (T2)	Reconstruction Error (T1)	Reconstruction Error (T2)
P01	PD	0.5092	0.4802	0.0290	7.8932	7.8402	0.0479	0.0572
P02	PD	0.5092	0.4919	0.0173	7.8935	7.8405	0.0480	0.0592
P03	PD	0.5055	0.4753	0.0302	7.8853	7.8265	0.0485	0.0618
P04	PD	0.5135	0.4828	0.0307	7.8690	7.8264	0.0475	0.0601
P05	PD	0.5043	0.4779	0.0264	7.8966	7.8365	0.0490	0.0677
P06	Normal	0.4872	0.4431	0.0441	7.8742	7.8237	0.0550	0.0609
P07	Normal	0.4718	0.4393	0.0325	7.8841	7.8184	0.0535	0.0649
P08	Normal	0.4467	0.4605	−0.0138	7.8618	7.8187	0.0500	0.0672
P09	Normal	0.5213	0.4533	0.0680	7.8778	7.8667	0.0507	0.0582
P10	Normal	0.4851	0.4372	0.0478	7.8839	7.8029	0.0510	0.0599

International Journal of
Medical Toxicology & Forensic Medicine



International Journal of
Medical Toxicology & Forensic Medicine

Figure 6. All 20 SCSR.

Stochastic Cortical Self-Reconstruction

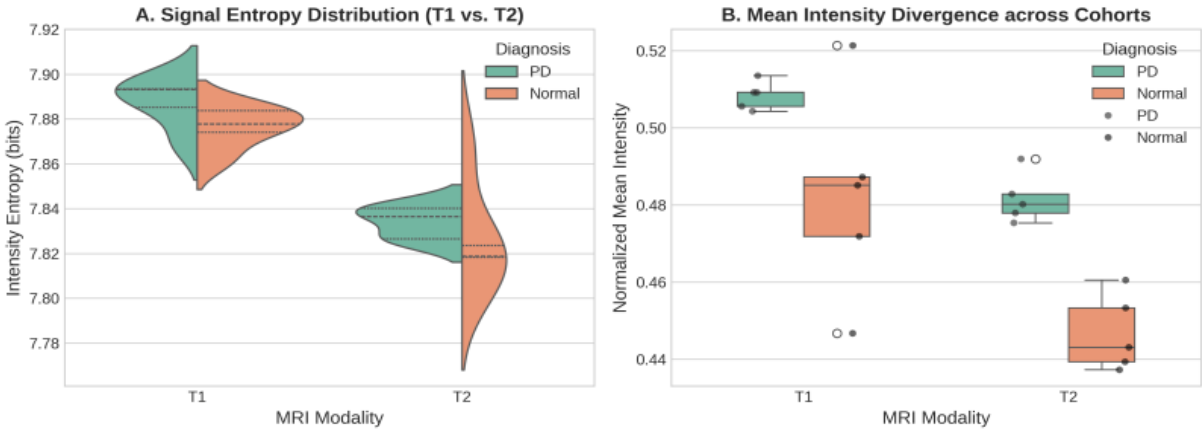
Figure 6 shows SCSR-reconstructed T1- and T2-weighted 3D MRI scans from 10 subjects (P01–P10), each with a resolution of 192 × 256 × 256 voxels. SCSR uses structural information from pre-processed MRI data to reconstruct cortical surfaces.

Figure 7 compares MRI intensity and entropy before data augmentation. T1 images show slightly higher entropy (7.85–7.91 bits) than T2 images (7.77–7.90 bits). The PD group has higher mean intensity with less variation, while normal group shows a wider intensity distribution with some outliers.

Patient-Specific Cortical Trajectories across Modalities

Table 1 presents representative patient-wise intensity, entropy, and reconstruction-error features extracted from T1- and T2-weighted MRI scans. These features illustrate the multimodal characteristics for distinguishing PD subjects from normal controls.

Differential Correlation and Biomarker Analysis



International Journal of
Medical Toxicology & Forensic Medicine

Figure 7. Intra-subject cortical mean trajectory.

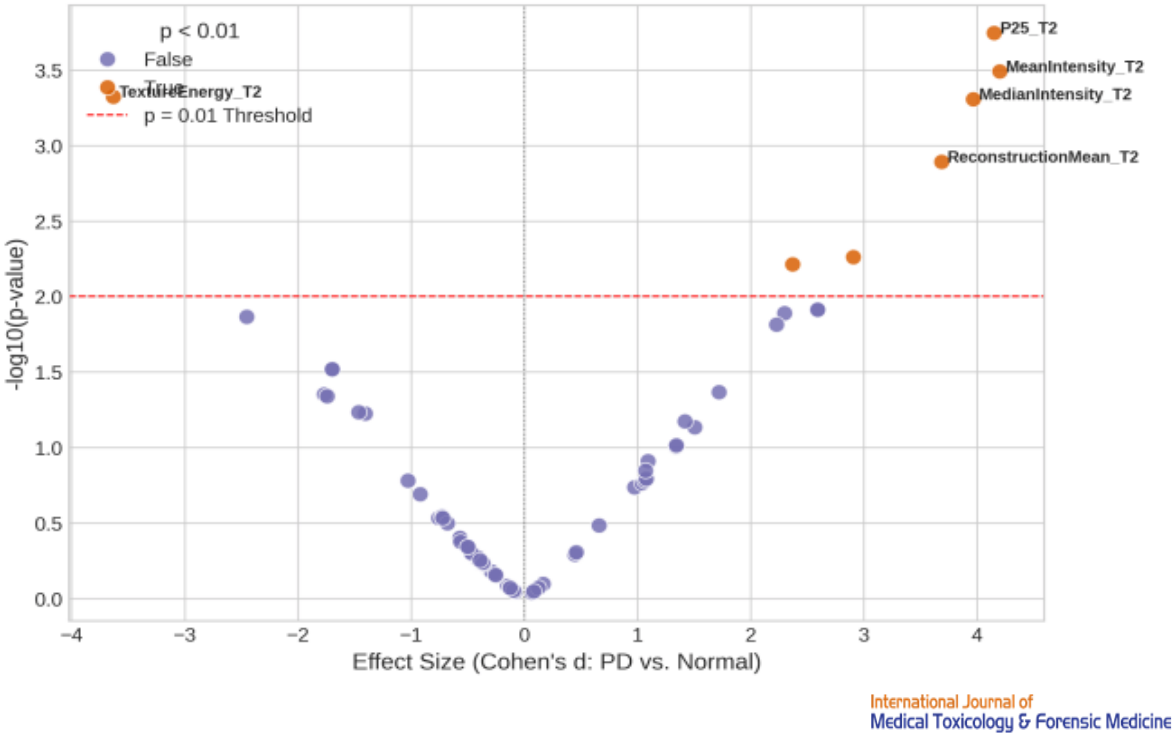


Figure 8. Redundancy matrix of differential features.

Figure 8 shows the correlations between different features (T1-T2). Slice Area Variation_Diff is strongly linked (r = 0.90) with related features. Median Intensity_Diff is closely related to Reconstruction Mean_Diff (r = 0.99), P75_Diff (r = 0.90), and P10_Diff (r = 0.90). P10_Diff and P25_Diff also have a strong link (r = 0.95). Gradient Mean_Diff is moderately connected with Gradient Std_Diff (r = 0.72), P75_Diff (r = 0.53), and P25_Diff (r = 0.52). Slice Mean Variation_Diff shows a negative link with P25_Diff (r = −0.80) and P10_Diff (r = −0.68). Inter Quartile Range_Diff has weak to moderate connections, meaning it adds unique info about intensity spread.

Discussion

Comparative Evaluation of Differential Biomarkers and PCA-Based Cohort Separability

Figure 9 shows the distributions of fused T1–T2 biomarkers for PD (green) and normal controls (orange). Brain Voxel Count Diff is statistically significant (p=0.0034). with PD median near -1.0×10^5 while normal controls show a wider distribution extending to -1.4×10^6.

Figure 10 shows PCA projection of multimodal

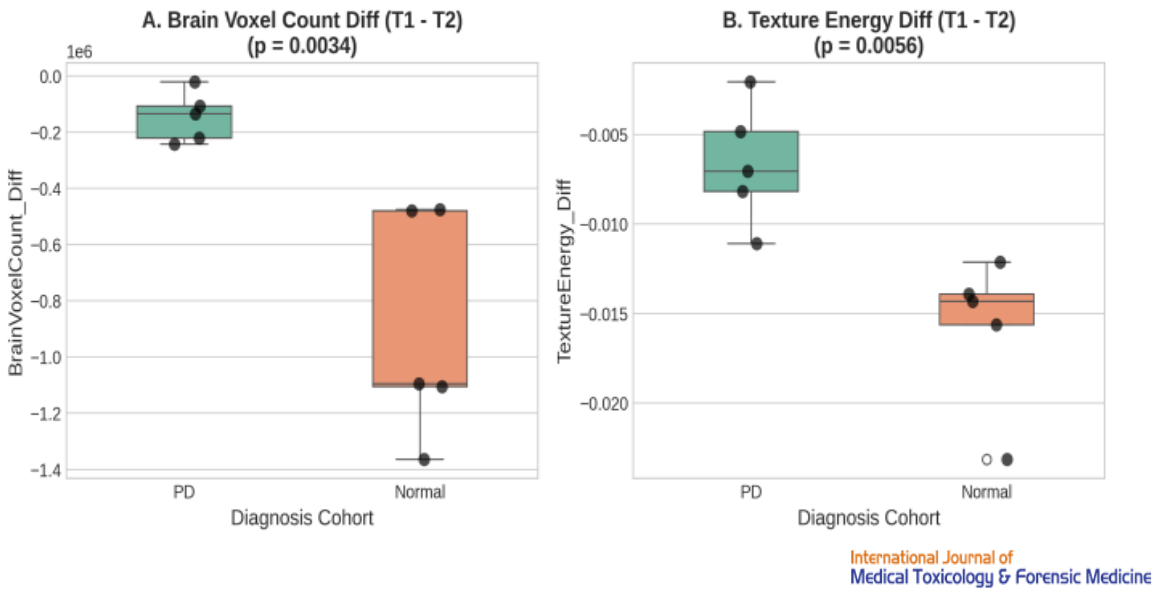


Figure 9. Statistical separation of key fused differential biomarkers.

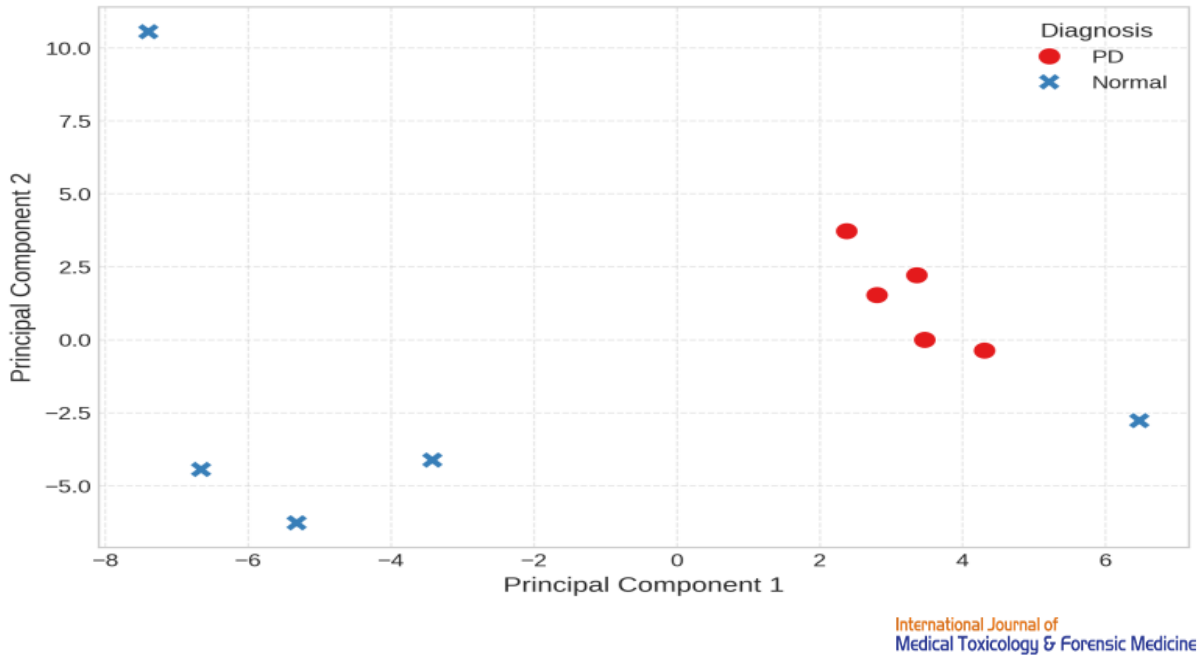


Figure 10. PCA cohort separation in fused feature space.

MRI features, with PC1 and PC2 explaining 34.3% and 31.3% of the variance, respectively. PD subjects form a cluster at positive PC1 values (+2.0 to +4.5), while normal controls cluster at negative values (−8.0 to −3.0), indicating clear separation between the groups.

Diagnostic Performance, Ablation Analysis and Biomarker Importance Analysis

Figure 11 shows ROC curves and ablation analysis with different feature configurations. T1-Only Model (Blue Dashed Line): Demonstrates high diagnostic capability with an Area Under the Curve of AUC = 0.92, using single-modality structural features. The T2-only and fused (T1 + T2 + Diff) models achieved an AUC of 1.00. The fused model reached a true positive rate of 1.0 at a false positive rate of 0.0, indicating clear group separation.

Figure 12 presents the top 15 MRI biomarkers ranked by RF Gini importance. MeanIntensity_T2 ranks highest (0.104), followed by TextureEnergy_T2 (0.083). Differential features, including brain volume, voxel count, texture energy, median intensity, and gradient mean, along with T1 intensity percentiles (P75_T1 and P90_T1), provide additional discriminatory information.

Table 2 rapid convergence the model shows sharp learning progression early on, with training accuracy jumping from 88.07% to 98.54% and loss dropping from 0.3447 to 0.0641 between Epochs 1 and 2. Stable Plateaus by Epoch 5, accuracy stabilizes near its peak

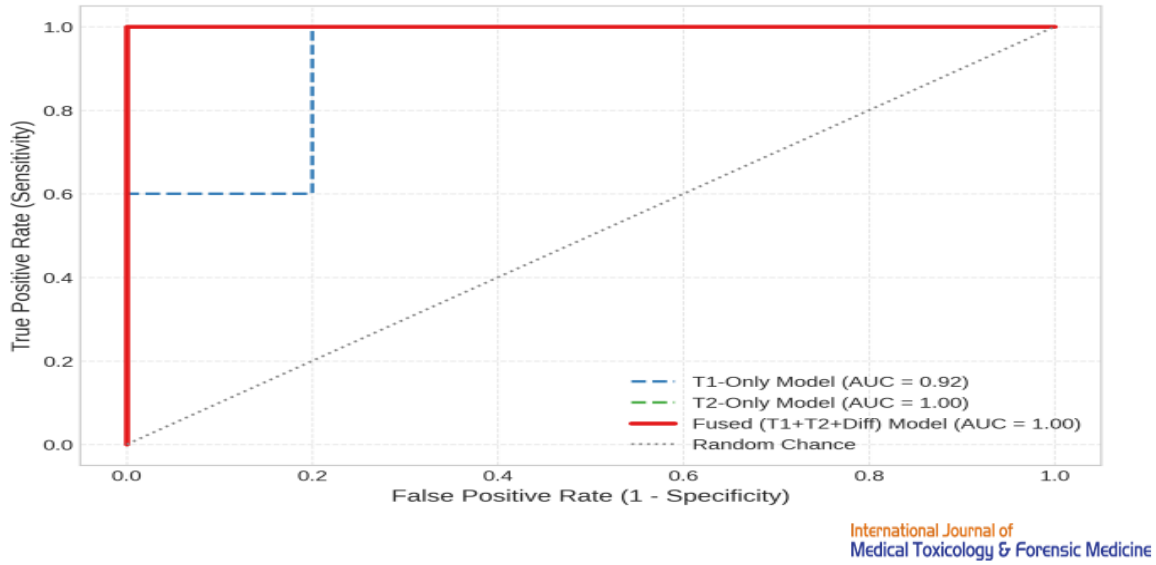
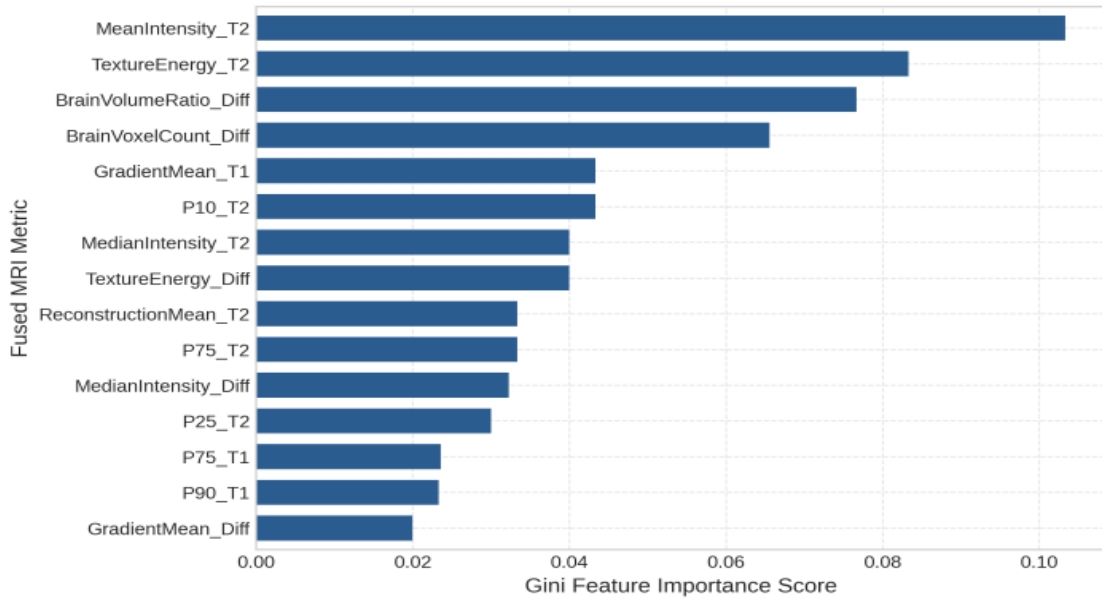


Figure 11. Ablation analysis - ROC diagnostic performance comparison.

Table 2. Epoch-wise training accuracy, loss, learning rate, and execution time.

Epoch	Training Accuracy (%)	Training Loss	Learning Rate	Training Time (s/Epoch)
1	88.07	0.3447	0.0010	869
2	98.54	0.0641	0.0010	801
3	98.94	0.0476	0.0010	795
4	99.12	0.0406	0.0010	787
5	99.14	0.0380*	0.0010	781

International Journal of Medical Toxicology & Forensic Medicine



International Journal of Medical Toxicology & Forensic Medicine

Figure 12. Top 15 discriminative biomarkers ranked by random forest.

at 99.14% with a minimized loss of 0.0380. Constant Learning Rate learning rate remains fixed at 0.0010 throughout all training steps.

Table 3 Superior Classification Performance Proposed Model (Stratified Boosted Learning) achieves a peak training accuracy of 99.14% and a precision of 96.0%, outperforming baseline works like Desai et al. (2024) (90.13%) and Cui et al. (2023)

Table 3. Comparative performance against recent literature.

Study	Dataset / NNN	Accuracy	Precision	Other reported values
Akgüller et al. (2024)	PPMI; N	NR	NR	Closeness: −22%; betweenness: −18%; network entropy: +15%; 10-fold CV
Bianco et al. (2026)	PD 219; HC 146; independent multi-site PPMI replication	NR	NR	Nested CV; no retraining for transfer result
Cui et al. (2023)	504 total; PD 255; HC 249	92%	NR	T2 MRI; PPMI
Desai et al. (2024)	NR	90.13%	NR	Augmentation gain: +15.53 percentage points
Dino & Hassan (2026)	PPMI; N	NR	NR	1.3M parameters; exact accuracy NR
Ezhilvendan & Raja (2026)	ADNI + PPMI + SchizConnect; N	NR	NR	Cross-dataset validation; exact PD-only metrics NR
Our Proposed Model (Stratified Boosted Learning)	**Multimodal 3D MRI / Custom**	**99.14%**	**96.0%**	**Final Loss: 0.0380; LR: 0.0010; 5 Epochs (781–869s/epoch)**

International Journal of Medical Toxicology & Forensic Medicine

(92%). Robust Convergence the model accomplishes this optimization efficiently within 5 epochs, reaching a final training loss of 0.0380 at a constant learning rate of 0.0010 and execution times ranging from 781 to 869 seconds per epoch.

Conclusion

This study presented a computational approach for analysing T1 and T2 MRI images using SCSR reconstruction and machine learning. The proposed method integrated volumetric, texture, and intensity features to distinguish patterns in the dataset. PCA showed that the first two components explained 65.6% of the total variance. Feature fusion achieved an AUC of 1.00, with MeanIntensity_T2 and TextureEnergy_T2 identified as important features. However, the results are preliminary due to the small cohort of 10 subjects. Further validation is required before considering clinical application. Future work will evaluate larger, multi-centre datasets, longitudinal MRI, and advanced deep learning methods to improve reliability, processing speed, and clinical applicability. Secure data transmission and hospital system integration will also be explored.

Ethical Approval

Not Applicable.

Acknowledgment

The authors thank all individuals who assisted with the conduct of the study.

Funding

No external funding was received for this research.

Conflicts of Interest

The authors report there are no competing interests to declare.

References

[1] Akan T, Akan S, Alp S, Ledbetter CR, Tafti AP, Arevalo O, et al. Deep Learning in neuroimaging for neurodegenerative diseases: State-of-the art, Challenges, and Opportunities. J Neurol Sci. 2025;478:123735. [DOI: 10.1016/j.jns.2025.123735]

[2] Akgüller Ö, Balcı MA, Cioca G. Functional Brain Network Disruptions in Parkinson's Disease: Insights from Information Theory and Machine Learning. Diagnostics (Basel). 2024;14(23):2728. [DOI: 10.3390/diagnostics14232728]

[3] Cui X, Chen N, Zhao C, Li J, Zheng X, Liu C, et al. An adaptive weighted attention-enhanced deep convolutional neural network for classification of MRI images of Parkinson's disease. J Neurosci Methods. 2023;394:109884. [DOI: 10.1016/j.jneumeth.2023.109884]

[4] Desai S, Chhinkaniwala H, Shah S, Gajjar P. Enhancing Parkinson's Disease Diagnosis through Deep Learning-Based Classification of 3D MRI Images. Procedia Comput Sci. 2024;235:201-13. [DOI: 10.1016/j.procs.2024.04.023]

[5] Islam NU, Khanam R. Machine learning based Parkinson's disease detection and progression evaluation using gray and white matter segmentation from 3D MRI. J Eng Appl Sci. 2024;71(1):65. [DOI: 10.1186/s44147-024-00522-7]

[6] Majhi B, Kashyap A, Mohanty SS, Dash S, Mallik S, Li A, et al. An improved method for diagnosis of Parkinson's disease using deep learning models enhanced with metaheuristic algorithm. BMC Med Imaging. 2024;24(1):241. [DOI: 10.1186/s12880-024-01335-z]

[7] Panahi M, Hosseini MS. Multi-modality radiomics of conventional T1 weighted and diffusion tensor imaging for differentiating Parkinson's disease motor subtypes in early-stages. Sci Rep. 2024;14(1):20492. [DOI: 10.1038/s41598-024-71860-y]

[8] Priyadharshini S, Ramkumar K, Vairavasundaram S, Narasimhan K, Venkatesh S, Amirtharajan R, et al. A Comprehensive framework for Parkinson's disease diagnosis using explainable artificial intelligence empowered machine learning techniques. Alexandria Eng J. 2024;107:568-82. [DOI: 10.1016/j.aej.2024.07.106]

[9] Sun Q, Wang F. Using artificial intelligence and radiomics to analyze imaging features of neurodegenerative diseases. Front Neurol. 2025;16:1624867. [DOI: 10.3389/fneur.2025.1624867]

[10] Parkinson's Progression Markers Initiative (PPMI). PPMI dataset. [Link]